Supplementary Information

Here, we would like to provide the supplementary information for our submitted manuscript entitled "Disentangling the impact of Atlantic Niño on sea-air CO_2 fluxes". Supplementary Information consists of discussion on the difference between the tropical Pacific and Atlantic, 1 table, 10 figures and reference list cited by Supplementary Information.

Discussion on the different mechanisms between Pacific and Atlantic:

Our results indicate that the sea-air CO_2 flux responds differently to the Atlantic Niño compared to its Pacific counterpart, the El Niño (Fig. 1). What is the reason behind these differences? Because the CO_2 flux anomalies in the Pacific are strongly related to the cold tongue associated with the upwelling, this difference is most likely a result of different carbonate composition of the Pacific and Atlantic deep waters. Supplementary Fig. S8 depicts a depth-longitude section of DIC and ALK. There is a steep vertical DIC gradient spanning the entire tropical Pacific and Atlantic from the surface to 200m depth. The modest ALK vertical gradient is limited to the continental shelf break at the eastern boundary in both basins, and also at the western boundary in the Atlantic. This indicates that the upwelling-induced DIC and ALK contributions to pCO_2 anomaly would be similar in both basins. Although the vertical gradient is similar, different responses in the pCO_2 could result from differences in the carbon buffering capacity, which is proportional to the carbonate ion (CO_3^{-2}) concentration. The CO_3^{-2} can be approximated from ALK minus DIC[S1]. Supplementary Fig.S9 shows the surface carbonate ion concentration in observational data and as simulated by the NorESM2. The tropical Pacific has a lower buffer capacity than the tropical Atlantic, primarily due to the evaporation-induced high alkalinity in the Atlantic. Since the pCO_2 change due to DIC ($dpCO_2$ / dDIC) is larger in the sea water with lower buffer capacity[35], the pCO_2 is more sensitive to the same DIC change in the tropical Pacific than in the tropical Atlantic. Supplementary Fig. S10 depicts the composite differences in CO_2 flux and each contribution to pCO_2 between Pacific El Niño and La Niña from NorESM2 simulation during November and December. In the central tropical Pacific, the salinity contribution is much less than the temperature (Supplementary Fig.S10b and c). Similar to the tropical Atlantic, the temperature anomaly enhances the upward CO_2 flux. The DIC contribution is much more dominant than the ALK contribution and the pCO_{2D_S} anomaly (-180 μatm) is much more pronounced than that in the tropical Atlantic (-70 μatm, Fig. 3f). In the case of the Pacific, the DIC contribution overwhelms the temperature contribution resulting in the reduction in CO_2 outflux at the equator (Supplementary Fig.S10a). On the other hand, the CO_2 flux anomaly is positive off the equator (Supplementary Fig.S10a), which is induced by the temperature. This positive anomaly is not seen in the observations and NorESM2 exhibits some bias off the equator. The CO_2 flux anomaly in the tropical Pacific can primarily be attributed to this DIC-driven pCO_2 change[S2] at the equator.

Name of calculartion \ Input data	SSS	SST	ALK	DIC	S-norm ALK	S-norm DIC	Silicate	Phosphate
pCO_{2F}	Monthly	Monthly	Monthly	Monthly	Not used	Not used	Climatology	Climatology
pCO_{2S}	Monthly	Climatology	Climatology	Climatology	Not used	Not used	Climatology	Climatology
pCO_{2T}	Climatology	Monthly	Climatology	Climatology	Not used	Not used	Climatology	Climatology
pCO_{2A}	Climatology	Climatology	Monthly	Climatology	Not used	Not used	Climatology	Climatology
pCO_{2D}	Climatology	Climatology	Climatology	Monthly	Not used	Not used	Climatology	Climatology
pCO_{2AD}	Climatology	Climatology	Monthly	Monthly	Not used	Not used	Climatology	Climatology
pCO_{2A_S}	Climatology	Climatology	Not used	Climatology	Monthly	Not used	Climatology	Climatology
pCO_{2D_S}	Climatology	Climatology	Climatology	Not used	Not used	Montly	Climatology	Climatology

Table S1.
List of pCO2 decomposition estimated from NorESM2 and the corresponding input varibales used in the CO2SYS module.
Name of each pCO_2 calculation with the CO2SYS module[20] in different combination of input data of the NorESM2 simulation. Except for SSS and SST, the data at first layer of the ocean component is utilized for the calculation. "S-norm" denotes the variable normalized by salinity (see the Method section for more details).

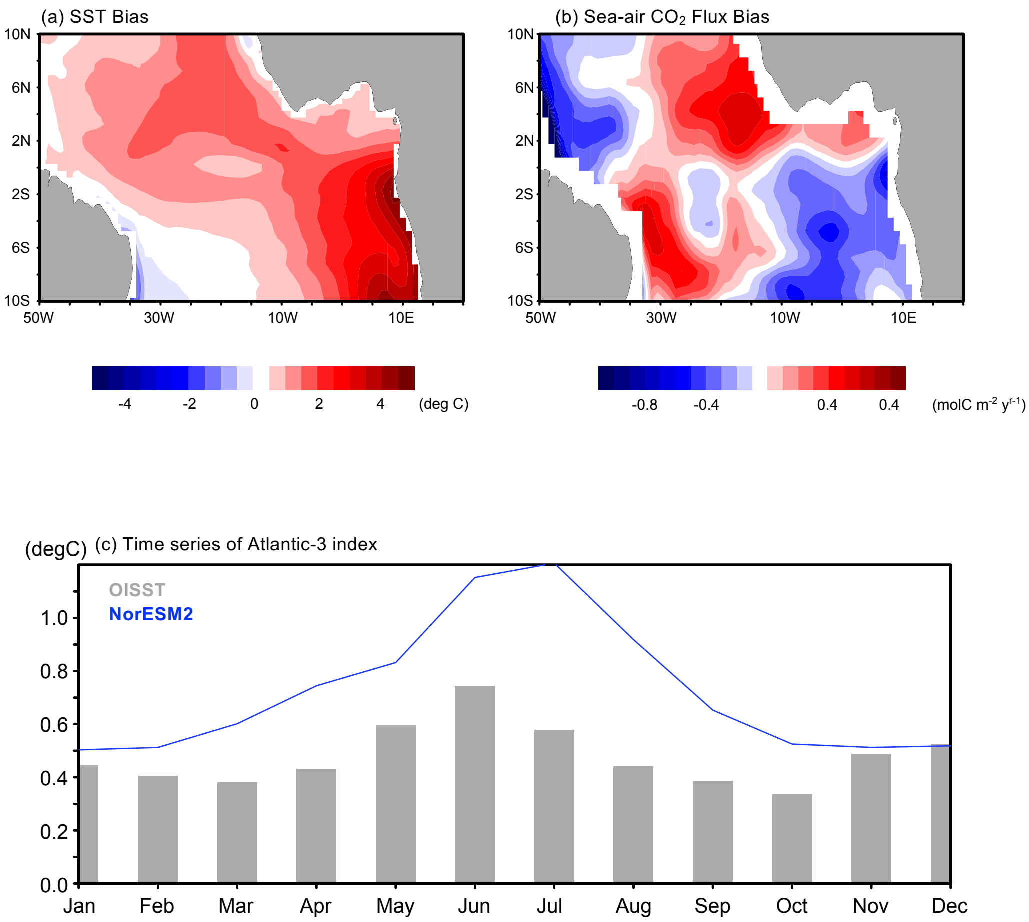

Figure S1.
Brief evaluation of NorESM2 with respect to observations.
June-July climatology bias of (a) sea surface temperature and (b) air-sea CO_2 flux for observation and NorESM simulations. Observed SST and CO_2 flux are obtained from OISST[S3] (1990-2019) and Landschützer et al. 2016[S4,S5] (1990-2015), respectively. (bottom) time series of Atlantic-3 index for observation (gray) and NorESM2 (blue), respectively.

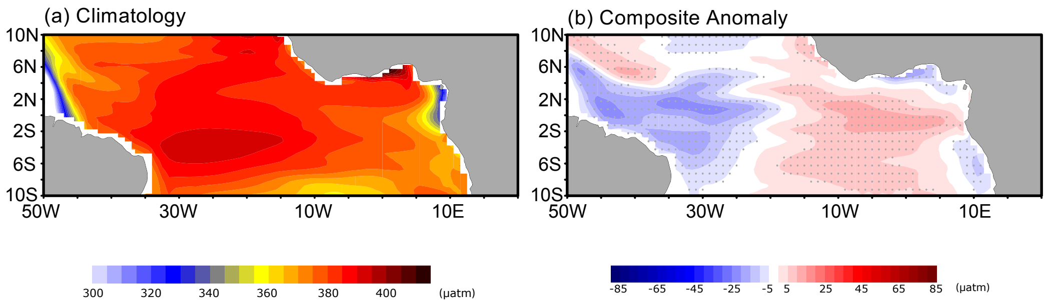

Figure S2.
NorESM-prognostic $p\mathrm{CO_2}$ cimatology and composite differece in $p\mathrm{CO_2}$ between Atlantic Niño and Niña

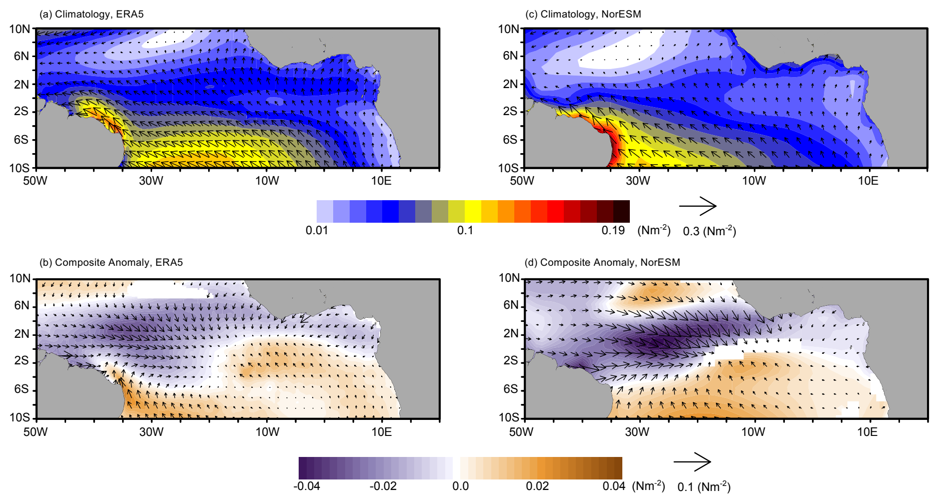

Figure S3.
Same as Fig.2, but for the (vectors) wind stress and (color) scalar of wind stress.
For reference to NorESM, ERA5 reanalysis[S6] data is utilized.

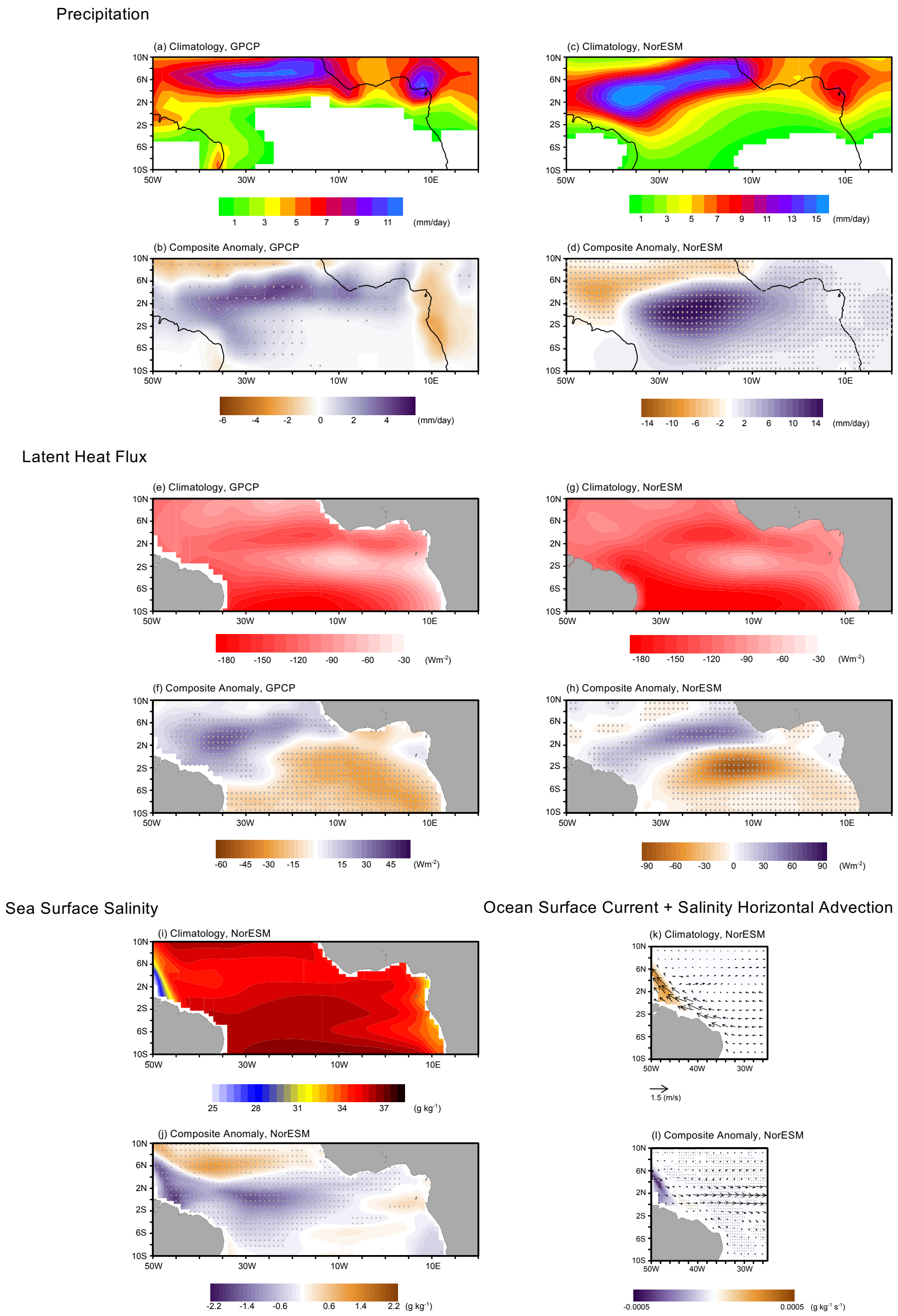

Figure S4.

Observed and NorESM-simulated climatology and composite anomalies relevant to freshwater.

Same as Fig. 2, but for the precipitation and latent heat flux for (left) observation and (right) NorESM simulation. The bottom panels are (left) sea surface salinity and (right) ocean surface current and salinity horizaontal advection from NorESM simulation. Note that observational sea surface salinity and ocean current monthly data with fine temporal duration is not available from 1990 to 2015. For the latent heat flux, negative denotes upward (ocean losses the heat and fresh water). Purplish (orangish) color for the anomalies indicates tendecy of desalitization (salitization) at the sea surface. Gray dots denote 90% (80% for Fig. 3l) of significance level and only vectors whose zonal or meridional component anomalies are significance (90%) are shown. The observation data are GPCP[S7] and TropFlux[S8] for precipitation and latent heat flux, respectively.

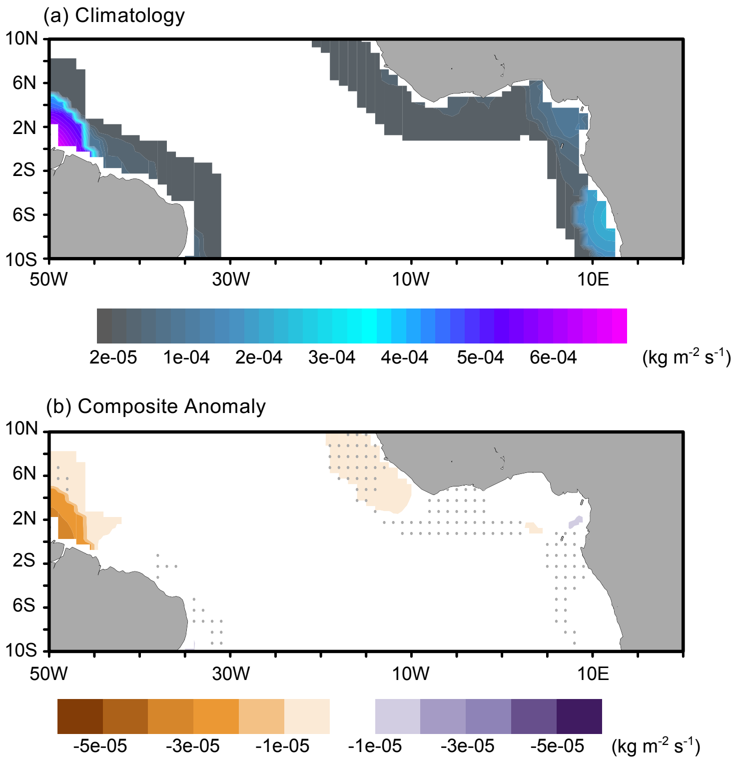

Figure S5.
Same as Fig.2, but for the river runoff of NorESM.

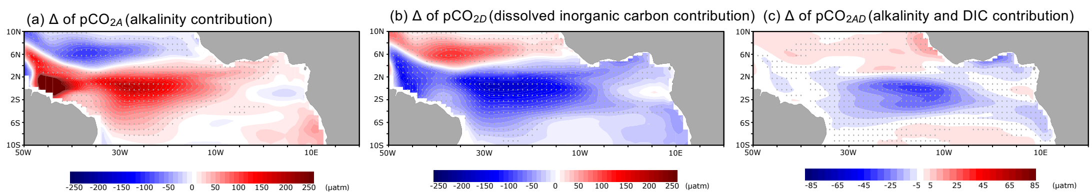

Figure S6.
Same as Fig.3, but for pCO_{2A}, pCO_{2D}, and pCO_{2AD}.

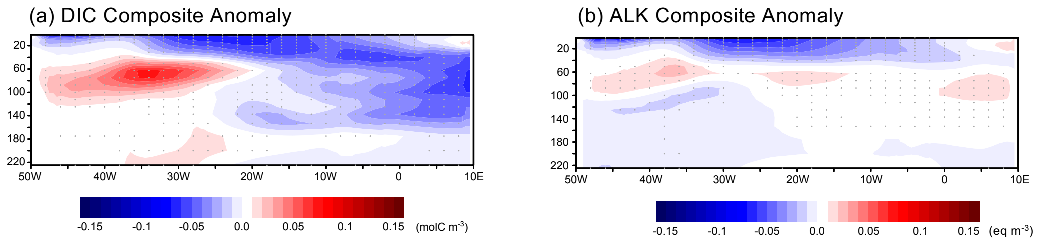

Figure S7.
Same as Fig.2, but for the vertical-longitude section of (left) dissolved inorganic carbon and (right) total alkalinity averaged between 2S and 4N.

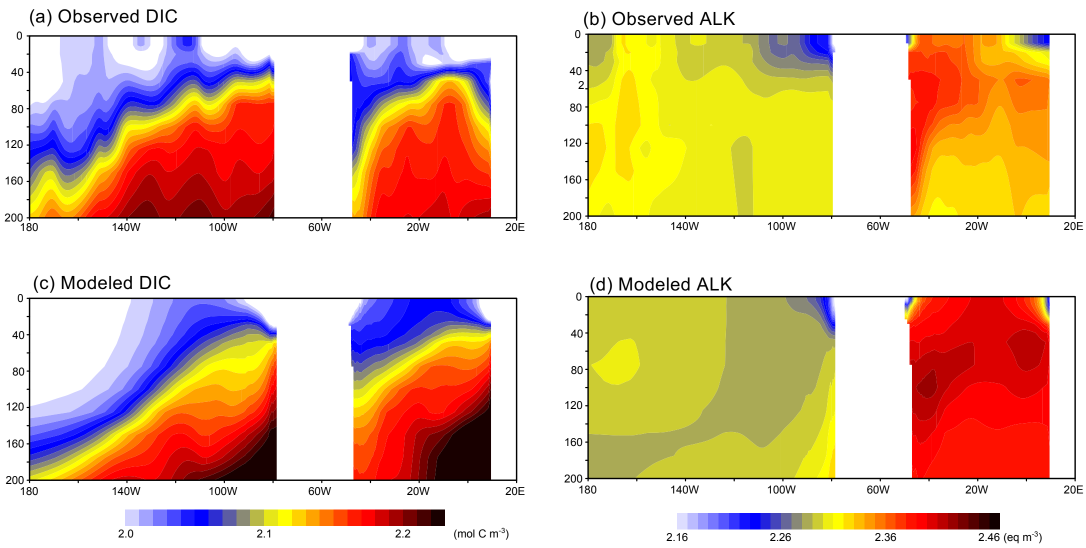

Figure S8
Depth-longitude section of annual-mean climatology of DIC and obtained from observation (top, GLODAP[S9]) and NorESM simulation (bottom) averaged 3°S and 3°N.

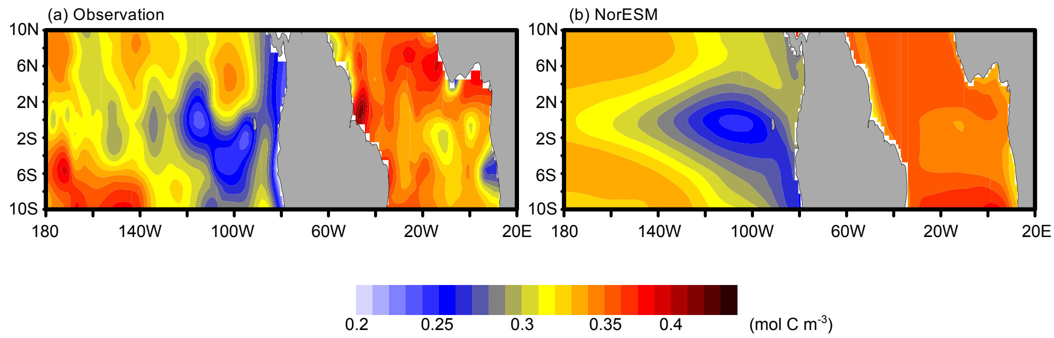

Figure S9.
Annual-mean climatology of carbonate ion[S1] (CO_3^{-2}) defined as ALK minus DIC at the surface for (a) observation[S9] and (b) NorESM2.

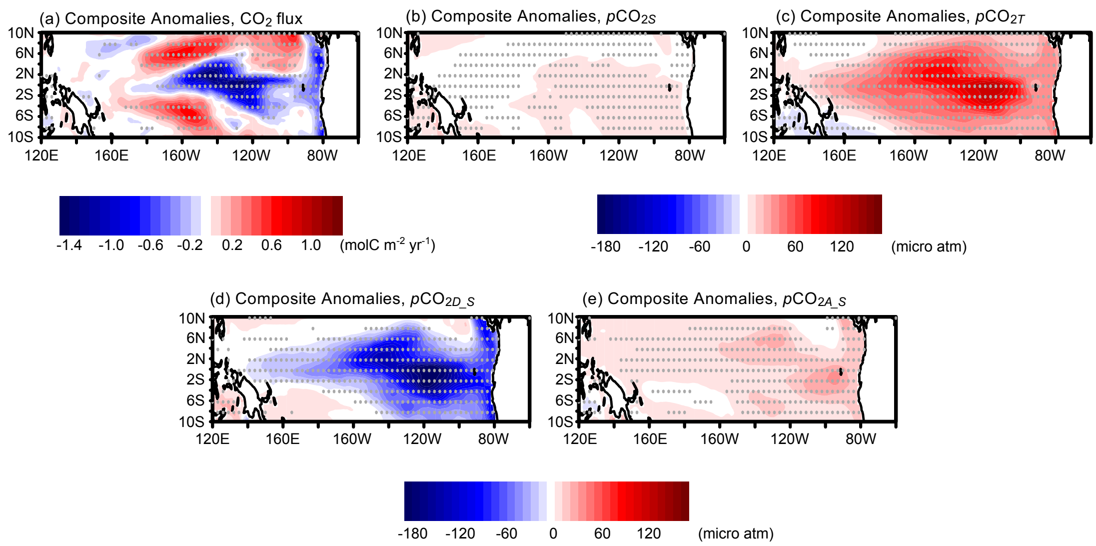

Figure S10.
Composite difference (defined as Δ)of (a) CO_2 flux, (b) pCO_{2S}, (c) pCO_{2T}, (d) pCO_{2D_S}, and (e) pCO_{2A_S} between El Niño and La Niña in November and December simulated by NorESM.

References for Supplementary Information

S1. Egleston, E. S., Sabine, C. L., and Morel, F. M. M., Revelle revisited: Buffer factors that quantify the response of ocean chemistry to changes in DIC and alkalinity. *Global Biogeochem. Cycles*, **24**, GB1002, doi:10.1029/2008GB003407, 2010.

S2. Feely, R. A., et al., Decadal variability of the air-sea CO_2 fluxes in the equatorial Pacific Ocean. *J. Geophy. Res. Oceans*, **111** (C8), https://doi.org/10.1029/2005JC003129. (2006)

S3. Reynolds, R. W., Smith, T. M., Liu, C., Chelton, D. B., Casey, K. S., & Schlax, M. G., Daily high-resolution-blended analyses for sea surface temperature. *J. Climate*, **20**, 5473-5496, doi:10.1175/JCLI-D-14-00293.1, (2007).

S4. Landschützer, P., Gruber, N., & Bakker, D. C. E., Decadal variations and trends of the global ocean carbon sink. *Global Biogeochem. Cycles*, **30**, 1396-1417, doi:10.1002/2015GB005359. (2016)

S5. Landschützer, P., Laruelle, G. G., Roobaert, A., & Regnier, P., 2020. A uniform pCO2 climatology combining open and coastal oceans. *Earth Syst. Sci. Data*, **12**, 2537-2553, https:/doi.org/10.5194/eesd-12-2537-2020. (2020).

S6. Hersbach, H., et al., The ERA5 global reanalysis. *Q. J. Roy. Meteorol. Soc.*, **146**, 1999-2049, https://doi.org/10.1002/qj.3803, 2020.

S7. Adler, R. F., Sapiano, M. R. P., Huffman, G. J., Wang, J.-J., Gu, G., Bolvin, D., Chiu, L., Schneider, U., Becker, A., Nelkin, E., Xie, P., Ferrano, R., & Shin D.-B., The Global Precipitation Climatology Project (GPCP) Monthly Analysis (New Version 2.3) and a Review of 2017 Global Precipitation. *Atmosphere*, **9**, 138, https:doi.org/10.3390/atmos9040138. 2018.

S8. Praveen Kumar, B., Vialard, J., Lengaigne, M., Murty, V. S. N., Mcphaden, M. J., Cronin, M. F., Pinsard, F., & Gopaka Reddy, K., TropFlux wind stress over the tropical oceans: evaluation and comparison with other products. *Clim. Dyn.*, **40** (7-8), 2049-2071.

S9. Lauvset, S. K., Key, R. M., Olsen, A., van Heuven, S., Velo, A., Lin, X., Schrnick, C., Kozyr, A., Tanhua, T., Hoppema, M., Jutterström, S. Steinfeldt, R., Jeansson, E., Ishii, M., Perez, F. F., Suzuki, T., & Watelet, S., A new global interior ocean mapped climatology: the 1°×1° GLODAP version 2. Earth Syst. Sci. Data, 8, 325-340, https://doi.org/10.5194/essd-8-325-2016 (2016)